Faraday Discussions

This paper is published as part of Faraday Discussions volume 143: Soft Nanotechnology

Introductory Lecture

Challenges in soft nanotechnology
Richard A. L. Jones, *Faraday Discuss.*, 2009
DOI: 10.1039/b916271m

Papers

Chemo and phototactic nano/microbots
Ayusman Sen, Michael Ibele, Yiying Hong and Darrell Velegol, *Faraday Discuss.*, 2009
DOI: 10.1039/b900971j

The efficiency of encapsulation within surface rehydrated polymersomes
A. J. Parnell, N. Tzokova, P. D. Topham, D. J. Adams, S. Adams, C. M. Fernyhough, A. J. Ryan and R. A. L. Jones, *Faraday Discuss.*, 2009
DOI: 10.1039/b902574j

Molecular control of ionic conduction in polymer nanopores
Eduardo R. Cruz-Chu, Thorsten Ritz, Zuzanna S. Siwy and Klaus Schulten, *Faraday Discuss.*, 2009
DOI: 10.1039/b906279n

Nanomechanics of organic/inorganic interfaces: a theoretical insight
Maria L. Sushko, *Faraday Discuss.*, 2009
DOI: 10.1039/b900861f

Discussion

General discussion
Faraday Discuss., 2009
DOI: 10.1039/b915402g

Papers

Solid state nanofibers based on self-assemblies: from cleaving from self-assemblies to multilevel hierarchical constructs
Olli Ikkala, Robin H. A. Ras, Nikolay Houbenov, Janne Ruokolainen, Marjo Pääkkö, Janne Laine, Markku Leskelä, Lars A. Berglund, Tom Lindström, Gerrit ten Brinke, Hermis Iatrou, Nikos Hadjichristidis and Charl F. J. Faul, *Faraday Discuss.*, 2009
DOI: 10.1039/b905204f

Nanoparticles at electrified liquid–liquid interfaces: new options for electro-optics
M. E. Flatté, A. A. Kornyshev and M. Urbakh, *Faraday Discuss.*, 2009
DOI: 10.1039/b901253m

Free-standing porous supramolecular assemblies of nanoparticles made using a double-templating strategy
Xing Yi Ling, In Yee Phang, David N. Reinhoudt, G. Julius Vancso and Jurriaan Huskens, *Faraday Discuss.*, 2009
DOI: 10.1039/b822156a

Polymer crystallization under nano-confinement of droplets studied by molecular simulations
Wenbing Hu, Tao Cai, Yu Ma, Jamie K. Hobbs, O. Farrance and Günter Reiter, *Faraday Discuss.*, 2009
DOI: 10.1039/b901378d

Nanostructured wrinkled surfaces for templating bionanoparticles—controlling and quantifying the degree of order
Anne Horn, Heiko G. Schoberth, Stephanie Hiltl, Arnaud Chiche, Qian Wang, Alexandra Schweikart, Andreas Fery and Alexander Böker, *Faraday Discuss.*, 2009
DOI: 10.1039/b902721a

Silica nano-particle super-hydrophobic surfaces: the effects of surface morphology and trapped air pockets on hydrodynamic drainage forces

Derek Y. C. Chan, Md. Hemayet Uddin, Kwun L. Cho, Irving I. Liaw, Robert N. Lamb, Geoffrey W. Stevens, Franz Grieser and Raymond R. Dagastine, *Faraday Discuss.*, 2009

DOI: 10.1039/b901134j

Discussion

General discussion

Faraday Discuss., 2009

DOI: 10.1039/b915406j

Papers

Counterion-activated polyions as soft sensing systems in lipid bilayer membranes: from cell-penetrating peptides to DNA

Toshihide Takeuchi, Naomi Sakai and Stefan Matile, *Faraday Discuss.*, 2009

DOI: 10.1039/b900133f

Recognition of sequence-information in synthetic copolymer chains by a conformationally-constrained tweezer molecule

Howard M. Colquhoun, Zhixue Zhu, Christine J. Cardin, Michael G. B. Drew and Yu Gan, *Faraday Discuss.*, 2009

DOI: 10.1039/b900684b

DNA self-assembly: from 2D to 3D

Chuan Zhang, Yu He, Min Su, Seung Hyeon Ko, Tao Ye, Yujun Leng, Xuping Sun, Alexander E. Ribbe, Wen Jiang and Chengde Mao, *Faraday Discuss.*, 2009

DOI: 10.1039/b905313c

Self-assembly of liquid crystal block copolymer PEG-*b*-smectic polymer in pure state and in dilute aqueous solution

Bing Xu, Rafael Piñol, Merveille Nono-Djamen, Sandrine Pensec, Patrick Keller, Pierre-Antoine Albouy, Daniel Lévy and Min-Hui Li, *Faraday Discuss.*, 2009

DOI: 10.1039/b902003a

A novel self-healing supramolecular polymer system

Stefano Burattini, Howard M. Colquhoun, Barnaby W. Greenland and Wayne Hayes, *Faraday Discuss.*, 2009

DOI: 10.1039/b900859d

Discussion

General discussion

Faraday Discuss., 2009

DOI: 10.1039/b915408f

Papers

Quantitative approaches to defining normal and aberrant protein homeostasis

Michele Vendruscolo and Christopher M. Dobson, *Faraday Discuss.*, 2009

DOI: 10.1039/b905825g

Evolving nanomaterials using enzyme-driven dynamic peptide libraries (eDPL)

Apurba K. Das, Andrew R. Hirst and Rein V. Ulijn, *Faraday Discuss.*, 2009

DOI: 10.1039/b902065a

Rational design of peptide-based building blocks for nanoscience and synthetic biology

Craig T. Armstrong, Aimee L. Boyle, Elizabeth H. C. Bromley, Zahra N. Mahmoud, Lisa Smith, Andrew R. Thomson and Derek N. Woolfson, *Faraday Discuss.*, 2009

DOI: 10.1039/b901610d

The influence of viscosity on the functioning of molecular motors

Martin Klok, Leon P. B. M. Janssen, Wesley R. Browne and Ben L. Feringa, *Faraday Discuss.*, 2009

DOI: 10.1039/b901841g

Template sol–gel synthesis of mesostructured silica composites using metal complexes bearing amphiphilic side chains: immobilization of a polymeric Pt complex formed by a metallophilic interaction

Wataru Otani, Kazushi Kinbara and Takuzo Aida, *Faraday Discuss.*, 2009

DOI: 10.1039/b904896k

Self-assembled interpenetrating networks by orthogonal self assembly of surfactants and hydrogelators

Aurelie M. Brizard, Marc C. A. Stuart and Jan H. van Esch, *Faraday Discuss.*, 2009

DOI: 10.1039/b903806j

Discussion

General discussion

Faraday Discuss., 2009

DOI: 10.1039/b915411f

Concluding remarks

Soft nanotechnology: ‘‘structure’’ vs. ‘‘function’’

George M. Whitesides and Darren J. Lipomi, *Faraday Discuss.*, 2009

DOI: 10.1039/b917540g

Silica nano-particle super-hydrophobic surfaces: the effects of surface morphology and trapped air pockets on hydrodynamic drainage forces

Derek Y. C. Chan,*[a] Md. Hemayet Uddin,[bc] Kwun L. Cho,[b] Irving I. Liaw,[b] Robert N. Lamb,[b] Geoffrey W. Stevens,[c] Franz Grieser[b] and Raymond R. Dagastine*[c]

Received 19th January 2009, Accepted 26th March 2009
First published as an Advance Article on the web 23rd July 2009
DOI: 10.1039/b901134j

We used atomic force microscopy to study dynamic forces between a rigid silica sphere (radius ~45 μm) and a silica nano-particle super-hydrophobic surface (SNP-SHS) in aqueous electrolyte, in the presence and absence of surfactant. Characterization of the SNP-SHS surface in air showed a surface roughness of up to two microns. When in contact with an aqueous phase, the SNP-SHS traps large, soft and stable air pockets in the surface interstices. The inherent roughness of the SNP-SHS together with the trapped air pockets are responsible for the superior hydrophobic properties of SNP-SHS such as high equilibrium contact angle (>140°) of water sessile drops on these surfaces and low hydrodynamic friction as observed in force measurements. We also observed that added surfactants adsorbed at the surface of air pockets magnified hydrodynamic interactions involving the SNP-SHS. The dynamic forces between the same silica sphere and a laterally smooth mica surface showed that the fitted Navier slip lengths using the Reynolds lubrication model were an order of magnitude larger than the length scale of the sphere surface roughness. The surface roughness and the lateral heterogeneity of the SNP-SHS hindered attempts to characterize the dynamic response using the Reynolds lubrication model even when augmented with a Navier slip boundary.

1. Introduction

The term "soft matter" has been used to describe a very broad range of materials from the synthetic to the biological with established and emerging applications. An important and unique property of soft matter materials is that their geometric deformations and the magnitude of their interactions with their environment have to be determined self-consistently. This requires knowing how soft matter deforms under external perturbations such as mechanical forces, hydrodynamic flow fields, electric fields, and osmotic pressure gradients from chemical species. Previously,

[a]*Department of Mathematics and Statistics, The Particulate Fluid Processing Centre, The University of Melbourne, Parkville, Victoria, 3010, Australia. E-mail: D.Chan@unimelb.edu.au*
[b]*School of Chemistry, The Particulate Fluid Processing Centre, The University of Melbourne, Parkville, Victoria, 3010, Australia*
[c]*Department of Chemical and Biomolecular Engineering, The Particulate Fluid Processing Centre, The University of Melbourne, Parkville, Victoria, 3010, Australia. E-mail: rrd@unimelb.edu.au*

we have focused on interactions involving drops and bubbles that are the basic building blocks in emulsions and foams to examine the coupling between geometric deformation to both equilibrium[1–8] and dynamic[9–20] forces on the nanometre scale. We also studied how adsorbed molecules at interfaces can modify these interactions by changing equilibrium surface forces and altering hydrodynamic boundary conditions of the flow field at liquid–liquid or liquid–gas interfaces.[9,11–13,19] This paper examines another type of soft material, a super-hydrophobic surface, where previous knowledge of the interactions between drops and bubbles is critically relevant to understanding nanometre scale interactions involving a super-hydrophobic surface in an aqueous environment.

Perhaps the most well-known example of a super-hydrophobic surface (SHS), commonly defined as any surface on which the contact angle of a sessile water drop is larger than 140°–150°,[21] is the lotus leaf.[22] Originally described by Cassie and Baxter,[21] it is the microstructure of the surface as well as the surface chemistry that impart super-hydrophobicity to the surface. The remarkable self-cleaning property of the lotus leaf has inspired a large number of approaches[23–25] to develop hierarchical or patterned surfaces to create synthetic super-hydrophobic surfaces to be used as anti-fouling coatings[26,27] and in novel applications in microfluidic devices.[28–30] Here we study dynamic interactions involving SHS made from silica nanoparticles (Fig. 1) that is being developed for use in anti-fouling coatings.[26,31,32] These SHS are of interest because their method of preparation is quite simple compared to processes involved in the manufacture of other types of SHS.[23–25] The microstructure of the surface of these materials have a high degree of porosity and roughness which impart to them the propensity to trap air within the porous coating in aqueous environments. Thus they have a unique combination of a rough and porous surface structure mixed with soft, trapped air bubbles in a single surface.

To investigate the dynamic behaviour of this soft matter material, we made use of atomic force microscopy (AFM) measurements and theoretical modelling of the dynamic interactions between these super-hydrophobic surfaces and a well-characterized rigid "probe" particle in aqueous solutions. We attempt to quantify the complex interplay between the hierarchical surface structure and the presence of trapped air within the coating that mediate the dynamic behaviour of this soft matter

Fig. 1 Two views of the same glass plate where the slightly opaque half has been made into a silica nano-particle super-hydrophobic surface; the clear half is uncoated glass. The drops of water, tinted in pink, have a high contact angle on the super-hydrophobic side but spread on the uncoated side.

coating by examining the dependence of the interactions with relative velocity, solution conditions and the types of molecules present. In this context, our previous work in AFM studies through novel force measurement methods and detailed modeling of the dynamic interactions in deformable systems is particularly relevant. Our initial studies focused on how equilibrium interactions affect droplet deformations[1–8,33] that complement the work of other researchers[34–38] and build on earlier studies on bubbles which had less detailed analysis.[39–43] More recent advances extended to the study of dynamic forces involving two drops[9,13–15,18] or a particle and a drop.[16,44] Earlier observations of dynamic deformations of a deformable mercury interface near a mica surface due to mechanical and electrical perturbations has also been modelled with quantitative success with the same theoretical framework.[19,20] The model also had success in predicting dynamic deformations in non-aqueous systems of glycerine in silicone oil[45] and has demonstrated that forces between deformable drops can be measured by simply measuring geometric deformations.[46] For all of the above, the observed hydrodynamic forces are consistent with the no-slip boundary conditions at solids and liquids interfaces.

Of particular relevance to the present work is our earlier studies of interactions involving bubbles[10–12] where, in the presence of surfactant, a no-slip boundary condition is observed whereas for a very clean air–water interface, the hydrodynamic boundary condition is more consistent with a Marangoni boundary condition rather than the no-slip condition. The dynamic interaction forces between a super-hydrophobic surface and a probe particle are expected to exhibit the effects of a combination of factors including the surface roughness, the hydrophobic character of the surface, and the presence of trapped bubbles with larger interfacial areas. This raises the question as to whether this combination of factors can be adequately captured under the single concept of 'slip'. However, what is clear is that the hierarchical nature of the surfaces requires careful characterization of the surfaces and the deployment of large colloid probes in the AFM measurement to maximize the magnitude of the interaction.

2. Materials and methods

2.1. Preparation of silica nano-particle super-hydrophobic surface (SNP-SHS)

The surfaces were prepared by spin-coating a solution of 40 nm silica nano-particles with methyltriacetoxysilane (MTAS) linker and polydimethylsiloxane (PDMS) in a hexane solvent on 1 mm thick, 2.54 cm diameter glass discs. The discs were baked in a furnace at 150 °C for 15 min. A more detailed description of the preparation methods can be found elsewhere.[31,32] The advancing contact angles of sessile drops of various aqueous solutions on these surfaces were measured using a Dataphysics OCA 20 tensiometer and goniometer system. For the 1 mM $NaNO_3$ solution the advancing and receding contact angles were $143° \pm 5°$ and $124° \pm 5°$, respectively, and for the 5 mM sodium dodecyl sulfate (SDS) solution the advancing and receding contact angles were $117° \pm 5°$ and $95° \pm 5°$, respectively. As these films were prepared by depositing hydrophobized nano-scale particles, the result is a surface with an extreme degree of roughness. The water contact angle of an equivalent smooth surface of the polysiloxane cross-linker was measured previously to be 75°.[26]

2.2. Method

The super-hydrophobic surfaces were imaged with an Asylum MFP-3D AFM (Asylum Research, Santa Barbara) both in air and in liquid with a closed fluid cell in AC mode. The cantilevers used for the imaging in air were rectangular silicon cantilevers (Budget Sensors, Sofia), and V-shaped non-conductive silicone nitride cantilever (Veeco, Santa Barbara) were used for AC mode in water. The cantilever and the SNP-SHS were cleaned in an ozone atmosphere for at least 20 min just before the imaging experiments. The liquid measurements were first performed

in 1 mM $NaNO_3$ aqueous solution. Then the substrate was washed with 30 ml of 20 mM SDS solution and the imaging was performed at approximately the same position on the sample in the same SDS solution three times over several hours.

For force measurements, a silica sphere of 45 ± 2 μm radius was attached to a custom-manufactured rectangular silicon AFM cantilever (dimensions: 450 μm × 50 μm × 2 μm) by using a two part epoxy adhesive.[47] The spring constant of the cantilever, K (0.2 ± 0.02 N m^{-1}) was determined by the thermal method.[48] The radius of the attached sphere was measured by video microscopy using a 50× objective. The surface roughness of the attached sphere was measured by a reverse image on a spiked grating (NT-MDT, Moscow) at the completion of the force measurements.

Force measurements were carried out using an Asylum MFP-3D AFM equipped with a linear variable displacement transducer (LVDT) in a closed fluid cell between a silica sphere and a freshly cleaved mica surface or a super-hydrophobic surface either in aqueous $NaNO_3$ or SDS solutions.

Force curves (an approach and retract force–distance cycle) were taken at a series of approach and retract piezo scan rates between 500 nm s^{-1} to 2 μm s^{-1} over a 70 μm × 70 μm scan area with 9 points on each line (a total of 81 force curves per force map). At higher speeds, up to 50 μm s^{-1}, the force curves were taken at manually selected 5 to 10 separate locations on the substrates. Results for the measured force normalised by the radius of the silica sphere were independent of the sphere size for larger spheres (35–50 μm), although there were irregularities with the smaller spheres (radius ~19 μm).

The deflection of the cantilever was converted from voltage signal to distance based on the constant compliance region (CCR) of force curves at slow (~1 μm s^{-1}) scan rates. The determination of the separation distance between the sphere and the surface using a CCR analysis has a number of difficulties for dynamic measurements. Further analysis of these data used an AFM force balance model that is discussed below.

3. Results

3.1. Surface characterization

3.1.1. Images of the silica nano-particle super-hydrophobic surface (SNP-SHS). Characterization of geometries involved in direct force measurements is a key requirement for quantitative comparison with theoretical models. In the case of super-hydrophobic surfaces with unusual surface morphology, characterization of the surfaces in air to visualize the intrinsic surface topography, as well as observation in liquid at the same aqueous solution conditions as the force measurement, is vital because of the possibility of trapped air bubbles on the surfaces. The addition of surfactant in the solution may also change the state of any trapped air on the super-hydrophobic surface, so visualization before and after the addition of surfactant in the same region is important.

3.1.2. In air. The topography of this type of super-hydrophobic surface is known to have significant surface roughness on the micrometre scale in the z-direction.[26] This was observed for the surfaces used in this study as well, where the roughness for different scan size images is given in Table 1. On a 50 × 50 μm scan the roughness scale is several micrometres. On the scale of several micrometres, the surface roughness is still of the order of half a micrometre. The surfaces also exhibit a large degree of lateral heterogeneity as shown in Fig. 2. Due to the large scale roughness of these samples, there may be some tip convolution effects when imaging the deepest valleys in air. As described below, these effects are less of an issue when imaged in liquid.

3.1.3. In aqueous solution. A series of AFM images for a SHS submerged in a 1 mM $NaNO_3$ electrolyte is given in Fig. 3 at successively higher magnifications.

Table 1 Average peak-to-valley roughness values of SNP-SHS from AFM images at a range of scan sizes

Scan size/μm	In air/μm	In 1 mM $NaNO_3$ electrolyte/μm
50 × 50	2.5	2.0
10 × 10	1.9	1.6
2 × 2	0.7	0.5

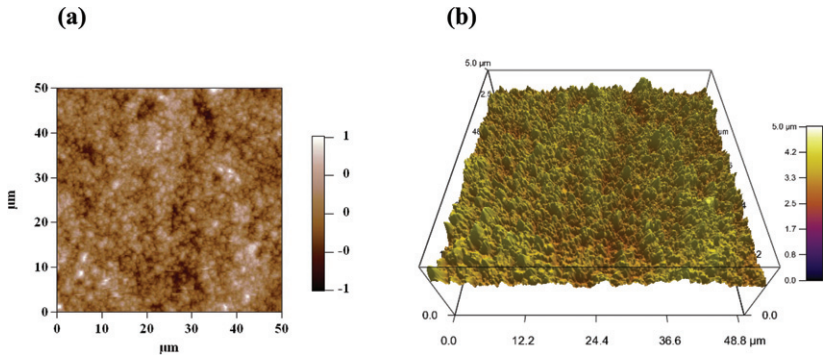

Fig. 2 AFM topography images of a silica nano-particle super-hydrophobic surface in air: (a) top view and (b) 3D view.

There are significant topographical differences compared to images in air, where the troughs and valleys of the images in air have been replaced by smooth interfaces of trapped air pockets that bridge the peaks of the surfaces. These features are visible regardless of magnification and these flat regions, with height variations of less than 2 nm, exhibit a clear and consistent contrast in the phase and amplitude images as well, indicating that these regions are not an artefact from tip convolution effects. When imaged at higher forces, these interfaces become depressed and then restore to their original height with a decrease in force. It is important to note the size of these air pockets is on the scale of hundreds of nanometres or smaller.

To investigate possible differences in the nature of the trapped air on the SNP-SHS in sodium nitrate and in SDS solutions, the same region was imaged before and after the addition of surfactant. These images are shown in Fig. 4 where a large bubble is also observed. The bubble appears to have a textured surface. This is an artefact of the imaging process, where the pressure from the tip deforms the bubble slightly by pressing on the topography underneath the air–water interface. Large bubbles of this size were observed in only about 10% of the 50 × 50 μm scans, whereas bubbles trapped within the peaks and valleys of the surface were observed in all scans. The addition of surfactant is expected to change the geometry of the bubble slightly as expected from adsorption of the SDS to the air–water interface (decreasing the surface tension from 72 mN m^{-1} to 39 mN m^{-1}), but the surfactant does not remove the trapped air from the SNP-SHS.

3.1.4. Silica sphere. This study employed a very rough sphere in the context of high precision AFM force measurements. It is well known that larger silica spheres can have significant roughness compared to smaller spheres, where a recent study also quantified this variability.[49] Reverse imaging of the sphere (radius ~45 μm) in air reveals a peak to trough roughness of approximately 22 nm and a similar root–mean–squared roughness over a 1 μm square region. This is significantly rougher than smaller silica spheres (radius ~5 μm) which commonly have

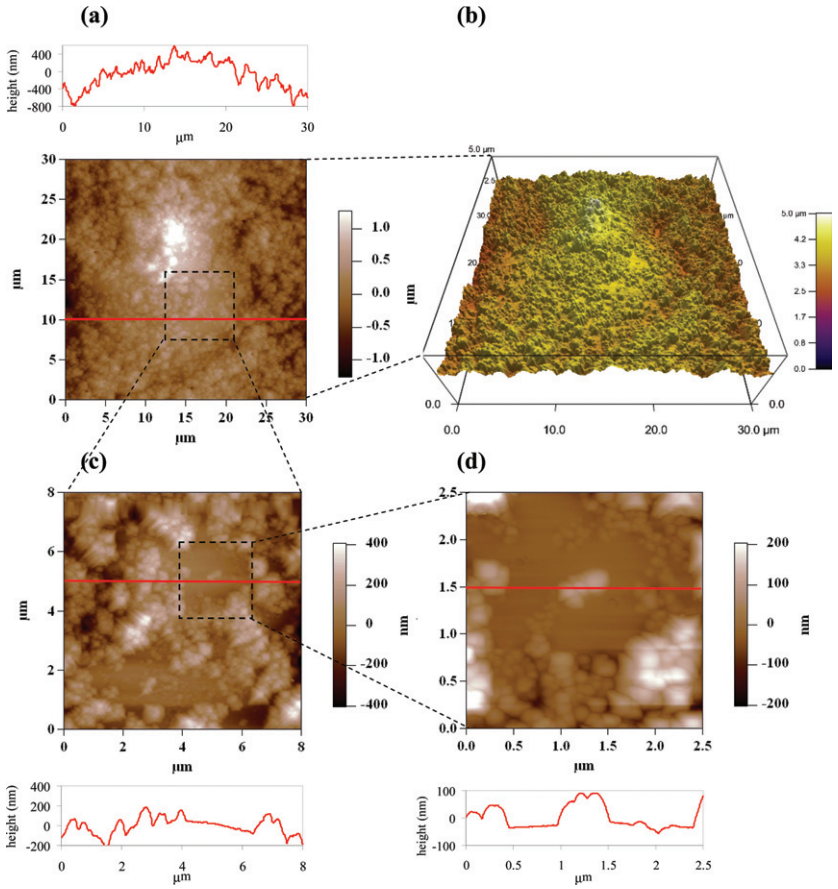

Fig. 3 AFM topography images of a silica nano-particle super-hydrophobic surface in 1 mM $NaNO_3$ aqueous solution: (a) top view and (b) 3D view with a scan size of 30 × 30 μm; (c) a zoomed in image of (a) with a scan size 8 × 8 μm; and (d) a zoomed in image of (c) with a scan size 2.5 × 2.5 μm. The solid lines on figures (a), (c) and (d) correspond to the cross-sections shown in the insets of the respective figures.

a root–mean–squared roughness under 3 nm.[49,50] The local curvature on this lateral scale is negligible due to the larger radius of the sphere.

3.2. Dynamic force measurements

In comparison to previous hydrodynamic drainage measurements on rigid surfaces, a larger sphere was used (radius ~45 μm) for several reasons. Both the sphere and the SNP-SHS have significant surface roughness. Surface roughness has been observed to decrease the hydrodynamic drainage force between a sphere and plate geometry measured using AFM.[51,52] In addition, previous studies using AFM often used additives such as sucrose to increase the viscosity of the solution and hence the magnitude of the hydrodynamic drainage force and experimentally accessible shear rates,[51,53,54] whereas this work was conducted without a viscosity modifier. In the regime of low Reynolds number lubrication hydrodynamics pertinent to the present experimental system, the hydrodynamic drainage force is expected to be linearly proportional to viscosity and has a quadratic dependence on the radius of the sphere for this geometry (see eqn (1)). In addition, the length scale of the surface roughness

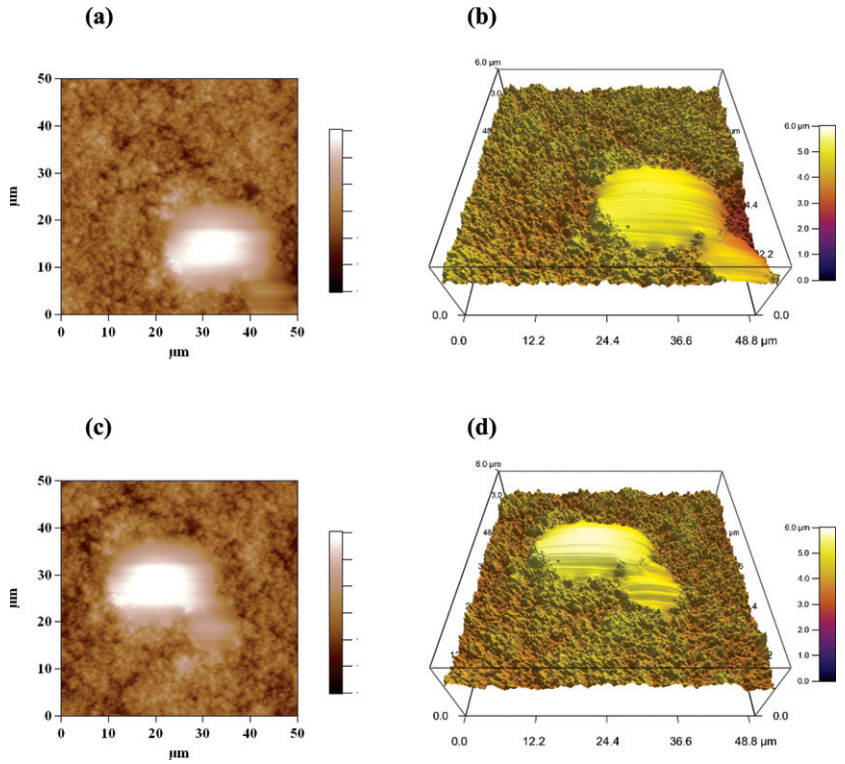

Fig. 4 AFM 50 × 50 μm scan size topography images of silica nano-particle super-hydrophobic surface in aqueous solutions: (a) top view in 1 mM $NaNO_3$ electrolyte; (b) 3D view of (a); (c) the same region of the surface after replacing the 1 mM $NaNO_3$ electrolyte with a 20 mM SDS; (d) 3D image of (c). The large egg-shaped feature in all images is a large air bubble on the surface. The lines on the bubble are scan line artefacts from the imaging process.

of the SNP-SHS and lateral heterogeneity are on the scale of micrometres, therefore the probe particle radius must be significantly larger than these length scales.

3.2.1. Silica sphere—mica surface. The large silica sphere has a non-negligible surface roughness. To isolate the effects of surface roughness of the large silica sphere prior to studying the SNP-SHS, the hydrodynamic drainage forces between the sphere and a model smooth surface, freshly cleaved mica, in aqueous solutions were examined. Typical dynamic force data as a function of time are shown in Fig. 5(a) at a series of increasing scan rates in 1 mM $NaNO_3$. The time axis for each scan rate has been scaled by β, the ratio between the scan rate and the lowest scan rate of the series. It is important to note this is a dynamic measurement and so all quantities such as the force, piezo position, separation and the velocity of the sphere are all parametric in time. The piezo velocity, dX_{LVDT}/dt, is not constant due to the non-linear motion of the piezo, but the LVDT records the actual position of the piezo with time which will be used directly in the analysis and model calculations. In addition, the velocity of the sphere will vary significantly with time in the proximity of the mica. The large hysteresis between the approach and retract curves and dependence of the force on approach and retract scan rate is clear. Both the magnitude of the repulsion on approach and the magnitude of the smoothly varying minimum upon retraction have a strong dependence on the piezo scan rate. The overall functional form of these data is similar to previous AFM measurements

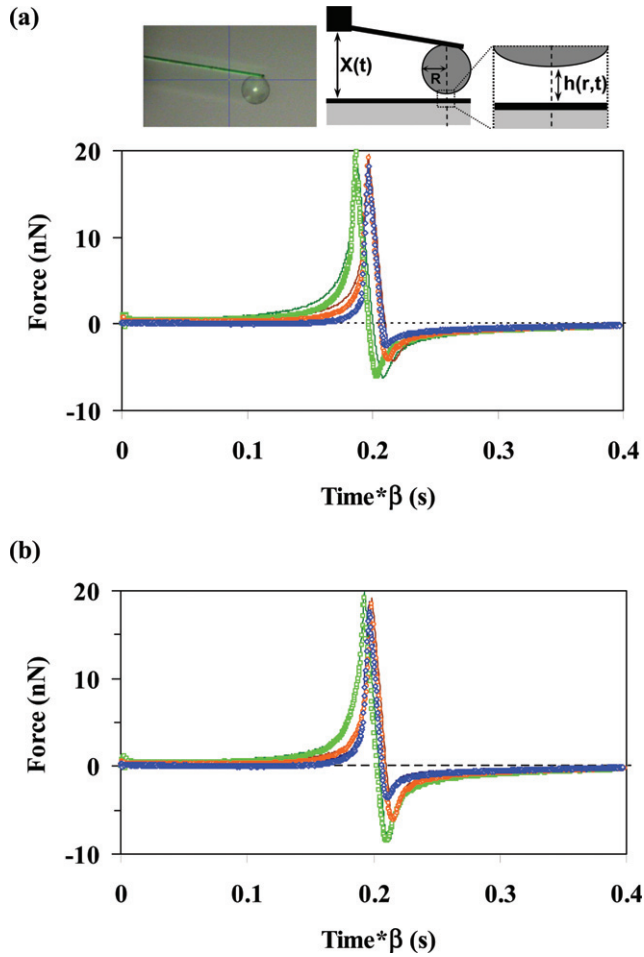

Fig. 5 Measured forces between a silica sphere (45 μm radius) and mica in aqueous solutions of (a) 1 mM $NaNO_3$ at average tip velocities of 11.8 (blue ◇), 23.3 (orange ○) and 34.5 (green □) μm s^{-1}; and (b) 20 mM SDS at average tip velocities of 11.7 (blue ◇), 23.4 (orange ○) and 35.1 (green □) μm s^{-1}. The time is scaled by a velocity ratio β ($\beta = V_h/V_1$, where V_h is 11.8, 23.3 and 34.5 μm s^{-1}, or 11.7, 23.4 and 35.1 μm s^{-1} and V_1 is 11.8 or 11.7 μm s^{-1} for (a) and (b), respectively). The solid lines in (a) and (b) correspond to an AFM force balance model fit to these data. The initial separation, $h(0)$, is determined from the fit. The $h(0)$ value from lowest to highest scan rates are 2300, 2300 and 2185 nm for (a) and 2256, 2275 and 2208 nm for (b). The insets in (a) show the photograph of the sphere attached on a rectangular cantilever and schematic diagram of the sphere–surface configuration showing the cantilever displacement function, $X(t)$; sphere radius, R; and separation, $h(r, t)$.

using smooth particles and flat surfaces.[51–54] A rigorous comparison to theory will be discussed below.

In the presence of a 20 mM SDS solution, dynamic force measurements were carried out using the same sphere and on the same sample in the same region as the measurements in Fig. 5(a). Typical results are shown in Fig. 5(b) and show a similar behaviour to Fig. 5(a). The electrical double layer forces are screened to a larger extent as the electrolyte concentration is an order of magnitude higher, the Debye length has decreased by two thirds and the surface potentials are expected to be lower (see Appendix). At this SDS concentration, adsorption of the SDS is not expected to either the mica surface or the silica surface as they are both negatively

charged,[55,56] so differences between the two measurements (Fig. 5(a) and (b)) are largely attributed to the differences in electrical double layer repulsion.

3.2.2. Silica sphere–silica nano-particle super-hydrophobic surface (SNP-SHS). The same silica sphere used in the measurements presented in Fig. 5 was used to measure the hydrodynamic forces between a sphere and SNP-SHS in the presence of 1 mM $NaNO_3$, 5 mM SDS and 20 mM SDS for a series of scan rates. Typical force data of measured forces *versus* time are shown in Fig. 6(a), (b) and (c) for these three solution conditions. In contrast to the mica data in Fig. 5, there is almost a complete absence of any speed dependent repulsion in Fig. 6(a) for the 1 mM $NaNO_3$ solution conditions and the absence of a smoothly varying hydrodynamic minimum in the retraction phase. Force measurements taken in the same region of the surface change significantly upon the exchange of 5 mM SDS for the $NaNO_3$ solution as shown in Fig. 6(b). The exchange of 20 mM SDS results in an additional increase of the dependence of the observed forces on scan rate shown in Fig. 6(c). The oscillations in the retraction curve are from a ringing in the piezo and tip holder that occur at high scan rates around the start of the retraction phase. This type of artefact has been observed previously in dynamic force measurement between rigid surfaces and is not expected to adversely affect the measurements.[53]

4. Discussion

4.1. Silica sphere–mica surface

Model comparison. The dynamic forces observed between the silica sphere and the mica surface have been compared to a force balance model of the AFM measurement that accounts for the electrical double layer forces between the silica and the mica, the motion of the cantilever in the AFM measurement, and the hydrodynamic drainage forces between the surfaces. Key points of the model are discussed below with the detailed description of the theory and relevant model equations provided in the Appendix. To describe the hydrodynamic drainage force between the two surfaces, the choice of the boundary condition of the velocity of the liquid adjacent to each surface is critical. The traditional assumption is that the tangential component of the velocity of the liquid at the surface is the same as that of the surface, commonly referred to as the no-slip boundary condition. Using Reynolds's lubrication theory, the hydrodynamic drainage force can be given by:

$$F_{\text{no-slip}} = -6\pi\mu R^2 \frac{1}{h}\frac{\mathrm{d}h}{\mathrm{d}t} \quad (1)$$

where μ is the dynamic viscosity, R is the radius of the sphere, h is the separation and t is time. A comparison between this no-slip model and experimental dynamic force data plotted as a function of time for mica–sphere interaction is shown in Fig. 7 for the 1 mM $NaNO_3$ case. The deviation observed between the calculations is typical for all of the data from Fig. 5(a) and (b) and is evidence that the hydrodynamic drainage force is significantly reduced from what is expected between two smooth surfaces following a no-slip boundary condition. In fitting the model to the force *versus* time data, the model is used to determine the mica–sphere separation.

This approach is significant as the determination of the separation between interacting surfaces is a key step in AFM force measurements. Traditionally, the force–displacement relation in the constant compliance region (CCR) is used to calibrate the instrument and to determine the location of hard contact and zero separation[57–59] for each force curve. However, for rough surfaces, hard contact occurs between the highest asperities of the surfaces and may lead to sliding or twisting of the cantilever upon further loading. In this work we use a static (low scan rate) measurement, to calibrate the instrument to process measurements at higher scan rates under similar

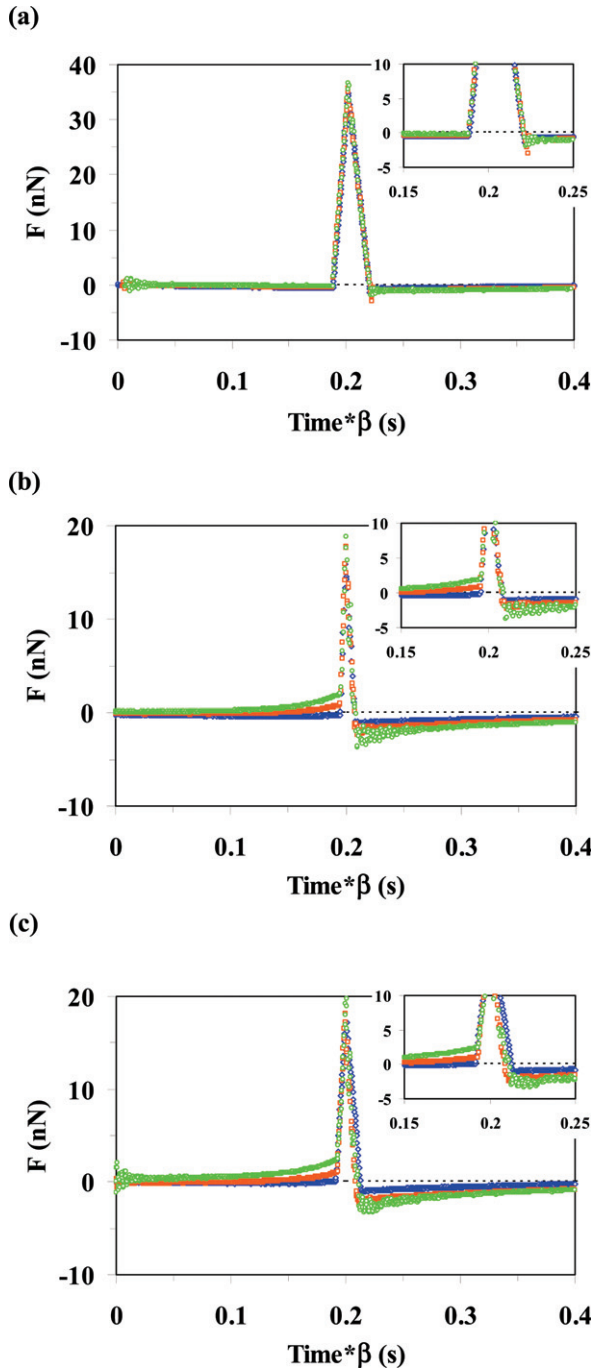

Fig. 6 Measured forces between a silica sphere (45 μm, radius) and a silica nano-particle superhydrophobic surface in aqueous solutions of (a) 1 mM $NaNO_3$ at average tip velocities of 11.9 (blue ◇), 35.0 (orange □) and 58.0 (green ○) μm s^{-1}; (b) 5 mM SDS at average tip velocities of 11.4 (blue ◇), 34.3 (orange □) and 57.3 (green ○) μm s^{-1}; and (c) 20 mM SDS at average tip velocities of 11.3 (blue ◇), 35.3 (orange □) and 55.5 (green ○) μm s^{-1}. The time is scaled by a velocity ratio β ($\beta = V_h/V_l$, where V_h is 11.9, 35.0 and 58.0 μm s^{-1}, or 11.4, 34.3 and 57.3 μm s^{-1}, or 11.3, 35.3 and 55.5 μm s^{-1} and V_l is 11.9 or 11.4 or 11.3 μm s^{-1} for (a), (b) and (c), respectively.

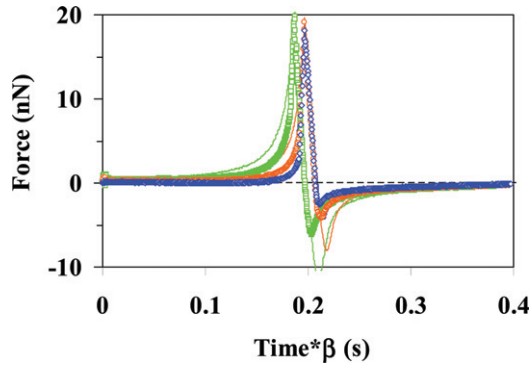

Fig. 7 A comparison of the measured forces between a silica sphere (45 μm radius) and mica in aqueous solutions of 1 mM $NaNO_3$ at average tip velocities 11.8 (blue ◇), 23.3 (orange ○) and 34.5 (green □) μm s^{-1} from Fig. 5(a) to an AFM force balance model using a no-slip boundary condition for the hydrodynamic drainage force. The solid lines are the model calculation. The time is scaled by a velocity ratio β ($\beta = V_h/V_l$, where V_h are 11.8, 23.3 and 34.5 μm s^{-1} and V_l is 11.8 μm s^{-1}).

conditions and use a hydrodynamic model to determine separation. Furthermore, previous force measurements of hydrodynamic drainage have had difficulties in determining the absolute separation that led to the conclusion that there is slip on a hydrophilic surface.[57,60,61] Recent AFM measurements that incorporated an evanescent wave scattering method to determine hard contact have shown that the observation of slip on hydrophilic surfaces measured using AFM to be an artefact.[54,62] Thus, the approach using force *versus* time may circumvent some of the above difficulties, depending on the accuracy of the hydrodynamic drainage model.

One approach to account for the effects of surface roughness on hydrodynamic drainage has been to use the Navier slip model and invoke the concept of a slip length, where the velocity of the liquid adjacent to a surface is assumed to be proportional to the shear stress at the surface.[51,52,63,64] The concept of a slip length in the context of thin film drainage[52,65–67] was originally proposed to explain deviations in hydrodynamic drainage forces for smooth surfaces but has also been used to characterise rough surfaces.[51,52] We compared our mica–sphere experiment results to a hydrodynamic drainage model that allows slip on one surface, in this case the silica sphere, as we know from independent experiments that the no-slip boundary condition is appropriate for the molecular mica surface.[11,68,69] The hydrodynamic drainage force for this model is given by

$$F_{\text{slip}} = -6\pi\mu R^2 \frac{f(h)}{h} \frac{\mathrm{d}h}{\mathrm{d}t} \tag{2}$$

where $f(h)$ is a function that allows for a slip length on one of the surfaces (see Appendix). The resulting comparisons of the model to the data for the 1 mM $NaNO_3$ and 20 mM SDS are given in Fig. 5(a) and (b), respectively. As the mica–surface separation is parametric in time, one can extract the variations of this separation from the resulting model fit. The fitted initial separation for each experiment, $h(0)$, are reported in Fig. 5. The incorporation of a slip model for the silica surface, has improved the agreement significantly, but there are still deviations as the force approaches the turn-around point, which occurs at small separations. The magnitude of the force data is consistent with the theoretical calculations, but the time position of the minimum in the forces is often predicted after the minimum in the data. Previous studies of hydrodynamic forces focused mainly on analysing the approach curves,[51,54] whereas the comparison in this work would suggest the

Table 2 The fitted Navier slip lengths for the silica sphere surface for silica–mica force data presented in Fig. 5

Speed[a]	11 μm s^{-1}	23μm s^{-1}	35μm s^{-1}
1 mM $NaNO_3$	90 nm	120 nm	120 nm
20 mM SDS	240 nm	325 nm	350 nm

[a] These are nominal velocities, exact value given in Fig. 5.

importance of examining the retraction curve as well to evaluate the accuracy of any model. The slip lengths for each system, $NaNO_3$ or SDS, given in Table 2 that fit each force curve varies by around ±10% over the range of scan rates examined. The magnitude of the slip lengths is much larger than the length scale (~20 nm) of the surface roughness of the silica sphere. The degree of agreement between experiments and predictions of the slip model and the deduced slip length can be affected by the extent that surface roughness can be described by the Navier slip model.

There have been recent advances in quantifying the effects of surface roughness on the measurement of static colloidal forces.[50,70,71] The most general consideration is that contact between rough surfaces is determined by the tallest asperities and therefore the magnitude of forces at contact will be reduced compared to those between smooth surfaces. In interpreting measurements of hydrodynamic forces between colloidal particles, the assumption of axisymmetric flow between smooth surfaces becomes problematic, particularly when the surface roughness becomes comparable to the mean separation, as in the case of the SNP-SHS in the present experiments.

Several studies have examined hydrophobic surfaces that were either chemically modified[52] or were polymeric surfaces[63,64] with intrinsic roughness. Only one AFM study has examined hydrophilic surfaces with rough surfaces by chemical modification of a silica surface.[51] The Navier slip model was used to interpret the measurements and the fitted slip lengths were also up to an order of magnitude larger than the length scale of the surface roughness where the previous study used a similar slip model. Vinogradova has proposed modifying the slip model by adding an additional parameter, which acts effectively as an offset in the separation, but this adds an additional fitting parameter to the model.[52] In addition, it is difficult to quantify the effects of random lateral heterogeneities that may give rise to low resistance lateral drainage pathways and hence reduce the magnitude of the hydrodynamic interaction relative to that between ideal smooth axisymmetric surfaces. Furthermore, even between surfaces with similar mean peak-to-trough roughness, the detailed surface topography can be quite different, so the lack of correlation between the deduced Navier slip length and the peak-to-trough roughness suggests that the model is at best empirical and a unified theory is yet to be developed.

4.2. Silica sphere–silica nano-particle super-hydrophobic surface (SNP-SHS)

The SNP-SHS possesses a surface roughness (~1–2 μm) several orders of magnitude greater than the silica sphere (~20 nm), which makes a detailed analysis of the hydrodynamic drainage force much more complicated. Indeed, the measured dynamic forces involving an SNP-SHS are significantly smaller than that involving mica and in some cases are almost undetectable. The approach used by previous researchers to interpret measured forces between a rough silica sphere and a smooth mica surface was to apply a Navier Slip model and treat the surface roughness as a perturbation to a smooth surface. The AFM images of the SNP-SHS indicate that the SNP-SHS roughness is extreme in comparison to the silica sphere and the surface itself is extremely porous. The SNP-SHS images in water do indicate that

the topography may appear flatter due to the presence of trapped air within the surface, but the surface roughness is still several hundred nanometres in range, even on a lateral scale of 1–2 μm. The large variations in lateral heterogeneity coupled with the magnitude of the roughness in the normal direction indicate that the axisymmetric lubrication model with smooth surfaces used for the silica sphere–mica system may not be extended to the SNP-SHS system.

The force data with the SNP-SHS exhibit some dynamic force behavior, but not for every solution condition. As described above, the forces with the SNP-SHS in the presence of $NaNO_3$ exhibit almost no dependence on scan rate, whereas the cases for 5 mM and 20 mM SDS show increases in the magnitude of a scan rate dependent force. To demonstrate that the forces in the SDS case arise from hydrodynamic drainage, the data from Fig. 6(a) and (c) were rescaled and plotted in Fig. 8. The cantilever deflection, which is proportional to the force, was divided by the average velocity and plotted against the same scaled time used in the insets of Fig. 6. For both Fig. 8(a) and (b) the approach points of the force curves roughly collapse on one another nearly forming a master curve. In the case of Fig. 8(a), the $NaNO_3$ case, there appears to be very little interaction, dynamic or static. In the case of the SDS in Fig. 8(b), this suggests that the deflection is dominated by hydrodynamic drainage effects. The variation in the overlap is primarily due to the variations in both starting separation and the variable nature of the rough SNP-SHS.

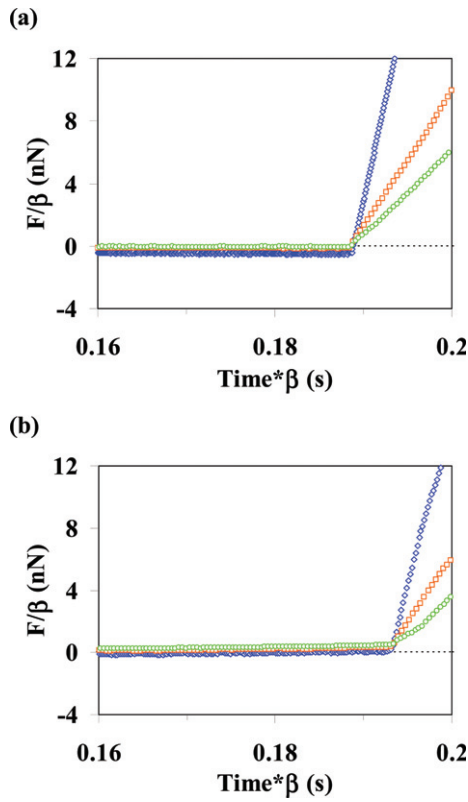

Fig. 8 Force *vs.* time curves for a silica sphere (45 μm, radius) and a silica nano-particle super-hydrophobic surface in aqueous solutions of (a) 1 mM $NaNO_3$ at average tip velocities of 11.9 (blue ◇), 35.0 (orange □) and 58.0 (green ○) μm s^{-1}; and (b) 20 mM SDS at average tip velocities of 11.3 (blue ◇), 35.3 (orange □) and 55.5 (green ○) μm s^{-1}. Both the force and time are scaled by a velocity ratio β ($\beta = V_h/V_l$, where V_h are 11.9, 35.0 and 58.0 μm s^{-1}, or 11.3, 35.3 and 55.5 μm s^{-1} and V_l is 11.9 or 11.3 μm s^{-1} for (a) and (b), respectively.

The SNP-SHS makes it difficult to develop further quantitative analysis using lubrication theory, but the rescaling of the SDS data and the lack of any dynamic effects in the absence of surfactant suggests that the trapped air in the SNP-SHS has an important role in affecting hydrodynamic drainage behavior. There are several possible reasons that the addition of surfactant can cause an increase in the drainage force. The first possible effect is from the change in shape and position of the air–water menisci of the many trapped air pockets on the SNP-SHS. As mentioned above, the contact angle of water on the SNP-SHS changes with surfactant present (from approximately 140° to 120°) as well as the change in surface tension with the addition of SDS. The AFM images before and after the addition of surfactant show that the trapped air is not removed, but the shape of the air–water menisci may change reducing some of the rough character of the surface. Both previous work and the measurements in this work on mica indicate that as surface roughness is reduced the hydrodynamic drainage forces will increase. Even with SDS in the system, the magnitudes of the dynamic forces are still considerably smaller than that observed for smooth surfaces such as mica.

The second possible reason for the changes in drainage behavior is from the boundary condition at the multitude of air–water menisci on the SNP-SHS. In the absence of any surface active materials the air–water interface is expected to match the velocity of the fluid adjacent to it, referred to as a completely mobile interface, which has the effect of significantly reducing the resistance to flow in the thin film between the sphere and the SNP-SHS. The addition of surface active materials at sufficiently high concentrations will saturate these interfaces, causing them to become immobile and result in an increase in the hydrodynamic drainage forces between the sphere and the SNP-SHS.

In our previous studies, we have been able to produce bubbles attached to an AFM cantilever with similar radii to the silica sphere in this work and examine the hydrodynamic drainage behavior during the velocity-dependent approach and retract above a mica plate.[10–12] In the presence of sufficient surfactant to saturate the air–water interface, the measured hydrodynamic forces change from the air–water interface being consistent with a partially mobile Marangoni surface to a no-slip surface. An example of the agreement between theory and measurement for the interaction forces between a bubble and flat mica plate is shown in Fig. 9 for a series of approach and retract scan rates. This result is consistent with what is expected for the case of a system with surfactant present and is consistent with our previous work studying the hydrodynamic interactions between oil droplets.[9,13–18]

Force measurements in the absence of any surfactants exhibited behavior that was intermediate between that of an air–water interface with a completely mobile

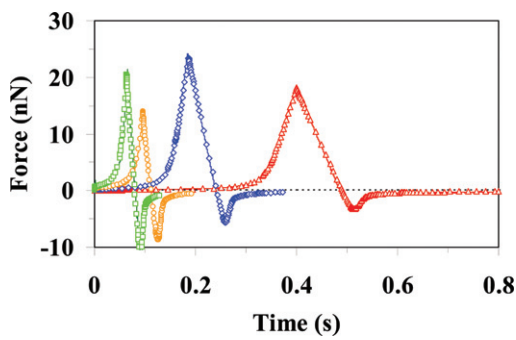

Fig. 9 Dynamic forces between a bubble and a mica plate in 10 mM SDS at tip velocities 5 (red △), 10 (blue ◇), 20 (orange ○) and 30 (□) μm s^{-1} and the model with no-slip boundary condition (solid lines).[11]

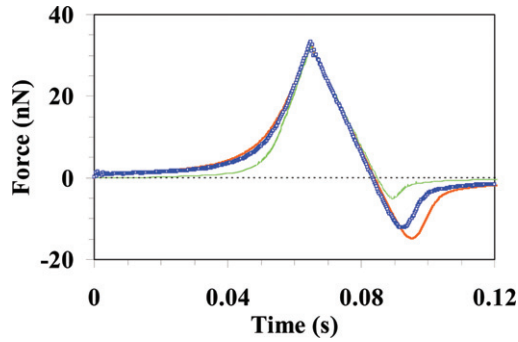

Fig. 10 Dynamic forces between a bubble and a mica plate in 1 mM $NaNO_3$ (no SDS) at tip velocity 30 μm s^{-1} (blue □) and the model with no-slip (solid line) and full-slip (dotted line) boundary conditions.[11]

interface and a completely immobile interface. An example of this is shown in Fig. 10. The observed force behavior was consistent with a partially mobile interface where both surface diffusion and convection were present due to the transport of ultra low levels of contaminants at the air–water interface. The authors proposed a method to model this quantitatively using a simple adsorption isotherm. These data and calculations demonstrate that on smooth surfaces the effects of surfactant can affect the hydrodynamic drainage forces in geometries of comparable sizes to this study by as much as fifty percent through altering the air–water boundary condition from a partially mobile interface to an immobile interface. The conclusion is that it is difficult to obtain air–water interfaces that are clean enough with such small surface areas to observe a fully mobile interface and this is consistent with difficulties in obtaining completely clean bubbles in bubble rise and bubble coalescence studies.[72–74]

The pronounced lack of drainage forces in the $NaNO_3$ solution and then increases in the magnitude of drainage forces with SDS solutions would suggest that the mobility of the air–water interfaces of the surface air pockets may play a significant role in the drainage behavior. It is worth noting that in the case of a SNP-SHS there is a large interfacial area of trapped air pockets such that contamination levels at the air–water interface may be quite low. Previous drainage studies by Charlaix and co-workers[75,76] between a millimetre size glass sphere and an order array of bubbles referred to as a "mattress of bubbles" have demonstrated the importance of the effects of a large number of bubbles at an air–liquid interface, but this study did not examine the effects of added surfactant and it employed viscosity modifiers with mixtures of water and glycerol. The added complexity of the SNP-SHS makes it difficult to identify if the geometric changes in the air–water interface are more or less important than an alteration of the flow boundary conditions at the air–water interfaces, but in either case the dynamic forces are clearly mediated by the presence and effect of surfactant on the air–water interface.

5. Conclusion

Surfaces that are used in practice that possess large scale surface roughness and heterogeneity can significantly reduce hydrodynamic effects that may dominate the dynamic interaction between relatively smooth surfaces. Previous work for hydrodynamic interactions between bubbles and surfaces has shown that the role of molecules at interfaces in changing hydrodynamic boundary conditions may be relevant to this SNP-SHS as well because of the presence of air pockets on such a surface. In addition the high degree of surface roughness of the SNP-SHS also

Table 3 System parameters for 1 mM $NaNO_3$ and 20 mM SDS

Parameter	Experimental	Model
Viscosity, μ/Pa s	10^{-3}	10^{-3}
Spring constant/N m^{-1}	0.20 ± 0.02	0.22
Mica surface potential ($NaNO_3$)[77]/mV	-80 ± 10	-80
Mica surface potential (SDS)[77]/mV	-70 ± 10	-70
Silica sphere surface potential ($NaNO_3$)[78]/mV	-50 ± 10	-50
Silica sphere surface potential (SDS)[78]/mV	-20 ± 10	-20
Radius of silica sphere/μm	45 ± 2	43

has an important role. One must use caution when attempting to extrapolate ideas gained about hydrodynamic drainage models developed for smooth surfaces to practical situations in either super-hydrophobic surfaces or even in other applications such as micro-fluidics, where surface roughness is often a key feature that is not well modeled by the concept of a simple Navier slip.

Appendix

The equation that governs the evolution of the separation, $h(t)$, between the silica sphere and the mica or super-hydrophobic surface is obtained by balancing forces on the sphere due to cantilever deflection, colloidal forces and hydrodynamic interaction. It has the form (see Fig. 5(a) in the inset):

$$\frac{dh}{dt} = \frac{h}{6\pi\mu R^2 f(h)}\left\{K[\Delta X(t) - h(t) + h(0)] + 2\pi R\, E(h)\right\} \tag{A1}$$

where

$$f(h) = \frac{1}{4}\left\{1 + \frac{3h}{2b}\left[\left(1 + \frac{h}{4b}\right)\log\left(1 + \frac{4b}{h}\right) - 1\right]\right\}$$

is the function that characterizes the hydrodynamic boundary condition of no-slip on the mica surface and Navier slip on the silica sphere[52,65] with slip length b. Interactions due to surface forces such as electrical double layer or van der Waals interactions are represented by the Deryaguin method in terms of the interaction energy per unit area, $E(h)$. The piezo displacement function $\Delta X(t)$ is taken from the LVDT output of the AFM. The cantilever deflection $[\Delta X(t) - h(t) + h(0)]$ can be obtained by solving eqn (A1) with a suitable choice of the initial separation, $h(0)$.

In our modeling we use the Poisson–Boltzmann theory to estimate the electrostatic repulsion for a given surface potential on each surface. van der Waals interactions are negligible for the range of separation encountered in our modeling.

The specific parameters used in modeling the fits in Fig. 4(a) and (b) are given below in Table 3.

References

1 R. R. Dagastine, D. C. Prieve and L. R. White, *J. Colloid Interface Sci.*, 2004, **269**, 84–96.
2 R. R. Dagastine and L. R. White, *J. Colloid Interface Sci.*, 2002, **247**, 310–320.
3 D. Y. C. Chan, R. R. Dagastine and L. R. White, *J. Colloid Interface Sci.*, 2001, **236**, 141–154.
4 L. Y. Clasohm, I. U. Vakarelski, R. R. Dagastine, D. Y. C. Chan, G. W. Stevens and F. Grieser, *Langmuir*, 2007, **23**, 9335–9340.
5 S. A. Nespolo, D. Y. C. Chan, F. Grieser, P. G. Hartley and G. W. Stevens, *Langmuir*, 2003, **19**, 2124–2133.

6 P. G. Hartley, F. Grieser, P. Mulvaney and G. W. Stevens, *Langmuir*, 1999, **15**, 7282–7289.
7 P. Mulvaney, J. M. Perera, S. Biggs, F. Grieser and G. W. Stevens, *J. Colloid Interface Sci.*, 1996, **183**, 614–616.
8 R. R. Dagastine, T. T. Chau, D. Y. C. Chan, G. W. Stevens and F. Grieser, *Faraday Discuss.*, 2005, **129**, 111–124.
9 G. B. Webber, S. A. Edwards, G. W. Stevens, F. Grieser, R. R. Dagastine and D. Y. C. Chan, *Soft Matter*, 2008, **4**, 1270–1278.
10 I. U. Vakarelski, J. Lee, R. R. Dagastine, D. Y. C. Chan, G. W. Stevens and F. Grieser, *Langmuir*, 2008, **24**, 603–605.
11 O. Manor, I. U. Vakarelski, X. Tang, S. J. O'Shea, G. W. Stevens, F. Grieser, R. R. Dagastine and D. Y. C. Chan, *Phys. Rev. Lett.*, 2008, **101**, 024501.
12 O. Manor, I. U. Vakarelski, G. W. Stevens, F. Grieser, R. R. Dagastine and D. Y. C. Chan, *Langmuir*, 2008, **24**, 11533–11543.
13 R. R. Dagastine, R. Manica, S. L. Carnie, D. Y. C. Chan, G. W. Stevens and F. Grieser, *Science*, 2006, **313**, 210–213.
14 S. L. Carnie, D. Y. C. Chan, C. Lewis, R. Manica and R. R. Dagastine, *Langmuir*, 2005, **21**, 2912–2922.
15 R. R. Dagastine, G. W. Stevens, D. Y. C. Chan and F. Grieser, *J. Colloid Interface Sci.*, 2004, **273**, 339–342.
16 G. B. Webber, R. Manica, S. A. Edwards, S. L. Carnie, G. W. Stevens, F. Grieser, R. R. Dagastine and D. Y. C. Chan, *J. Phys. Chem. C*, 2008, **112**, 567–574.
17 R. Manica, J. N. Connor, R. R. Dagastine, S. L. Carnie, R. G. Horn and D. Y. C. Chan, *Phys. Fluids*, 2008, **20**, 032101.
18 S. L. Carnie, D. Y. C. Chan and R. Manica, *ANZIAM J.*, 2005, **46**(E), C805–C819.
19 R. Manica, J. N. Connor, L. Y. Clasohm, S. L. Carnie, R. G. Horn and D. Y. C. Chan, *Langmuir*, 2008, **24**, 1381–1390.
20 R. Manica, J. N. Connor, S. L. Carnie, R. G. Horn and D. Y. C. Chan, *Langmuir*, 2007, **23**, 626–637.
21 A. B. D. Cassie and S. Baxter, *Trans. Faraday Soc.*, 1944, **40**, 546–551.
22 W. Barthlott and C. Neinhuis, *Planta*, 1997, **202**, 1–8.
23 R. Fuerstner, W. Barthlott, C. Neinhuis and P. Walzel, *Langmuir*, 2005, **21**, 956–961.
24 X. Zhang, F. Shi, J. Niu, Y. Jiang and Z. Wang, *J. Mater. Chem.*, 2008, **18**, 621–633.
25 P. Roach, N. J. Shirtcliffe and M. I. Newton, *Soft Matter*, 2008, **4**, 224–240.
26 H. Zhang, R. Lamb and J. Lewis, *Sci. Technol. Adv. Mater.*, 2005, **6**, 236–239.
27 J. Genzer and K. Efimenko, *Biofouling*, 2006, **22**, 339–360.
28 A. Chunder, K. Etcheverry, G. Londe, H. J. Cho and L. Zhai, *Colloids Surf., A*, 2009, **333**, 187–193.
29 F.-M. Chang, Y.-J. Sheng, S.-L. Cheng and H.-K. Tsao, *Appl. Phys. Lett.*, 2008, **92**, 264102.
30 J. Hyvaluoma and J. Harting, *Phys. Rev. Lett.*, 2008, **100**, 246001.
31 H. Zhang and R. N. Lamb, *PCT Int. Appl.*, 2005, p. 36.
32 R. N. Lamb, H. Zhang and C. L. Raston, *PCT Int. Appl.*, 1998, p. 20.
33 R. R. Dagastine and G. W. Stevens, in *Interfacial Nanochemistry: Molecular Science and Engineering at Liquid–Liquid Interfaces*, ed. H. Watarai, N. Teramae and T. Sawada, Kluwer Academic, New York, 2005, pp. 77–95.
34 G. Gillies, C. A. Prestidge and P. Attard, *Langmuir*, 2002, **18**, 1674–1679.
35 D. E. Aston and J. C. Berg, *J. Colloid Interface Sci.*, 2001, **235**, 162–169.
36 B. A. Snyder, D. E. Aston and J. C. Berg, *Langmuir*, 1997, **13**, 590–593.
37 A. P. Gunning, A. R. Mackie, P. J. Wilde and V. J. Morris, *Langmuir*, 2004, **20**, 116–122.
38 D. Bhatt, J. Newman and C. J. Radke, *Langmuir*, 2001, **17**, 116–130.
39 W. A. Ducker, Z. Xu and J. N. Israelachvili, *Langmuir*, 1994, **10**, 3279–3289.
40 M. Preuss and H.-J. Butt, *Langmuir*, 1998, **14**, 3164–3174.
41 G. Gillies, M. Kappl and H.-J. Butt, *Adv. Colloid Interface Sci.*, 2005, **114–115**, 165–172.
42 M. L. Fielden, R. A. Hayes and J. Ralston, *Langmuir*, 1996, **12**, 3721–3727.
43 N. Yap, D. Feng, R. R. Dagastine, G. C. Lukey and J. S. J. van Deventer, *Publ. Australas. Inst. Min. Metall.*, 2005, **5/2005**, 643–649.
44 D. E. Aston and J. C. Berg, *Ind. Eng. Chem. Res.*, 2002, **41**, 389–396.
45 R. Manica, E. Klaseboer and D. Y. C. Chan, *Soft Matter*, 2008, **4**, 1613–1616.
46 D. Y. C. Chan, O. Manor, J. N. Connor and R. G. Horn, *Soft Matter*, 2008, **4**, 471–474.
47 W. A. Ducker, T. J. Senden and R. M. Pashley, *Nature*, 1991, **353**, 239–241.
48 J. L. Hutter and J. Bechhoefer, *Rev. Sci. Instrum.*, 1993, **64**, 1868–1873.
49 P. J. van Zwol, G. Palasantzas, M. van de Schootbrugge, J. T. M. de Hosson and V. S. J. Craig, *Langmuir*, 2008, **24**, 7528–7531.
50 R. R. Dagastine, M. Bevan, L. R. White and D. C. Prieve, *J. Adhes.*, 2004, **80**, 365–394.
51 E. Bonaccurso, H.-J. Butt and V. S. J. Craig, *Phys. Rev. Lett.*, 2003, **90**, 144501.

52 O. I. Vinogradova and G. E. Yakubov, *Phys. Rev. E: Stat., Nonlinear, Soft Matter Phys.*, 2006, **73**, 045302.
53 C. D. F. Honig and W. A. Ducker, *Phys. Rev. Lett.*, 2007, **98**, 028305.
54 C. Neto, V. S. J. Craig and D. R. M. Williams, *Eur. Phys. J. E*, 2003, **12**, 71–74.
55 J. Penfold, E. Staples, I. Tucker and R. K. Thomas, *Langmuir*, 2002, **18**, 5755–5760.
56 J. C. Schulz and G. G. Warr, *Langmuir*, 2000, **16**, 2995–2996.
57 E. Bonaccurso, M. Kappl and H.-J. Butt, *Curr. Opin. Colloid Interface Sci.*, 2008, **13**, 107–119.
58 T. J. Senden, *Curr. Opin. Colloid Interface Sci.*, 2001, **6**, 95–101.
59 I. M. Nnebe, R. D. Tilton and J. W. Schneider, *J. Colloid Interface Sci.*, 2004, **276**, 306–316.
60 C. Neto, D. R. Evans, E. Bonaccurso, H.-J. Butt and V. S. J. Craig, *Rep. Prog. Phys.*, 2005, **68**, 2859–2897.
61 E. Lauga, M. P. Brenner and H. A. Stone, in *Handbook of Experimental Fluid Dynamics*, ed. J. Foss, C. Tropea and A. Yarin, Springer, New York, 2005.
62 E. Bonaccurso, M. Kappl and H.-J. Butt, *Phys. Rev. Lett.*, 2002, **88**, 076103.
63 R. Pit, H. Hervet and L. Léger, *Phys. Rev. Lett.*, 2000, **85**, 980–983.
64 Y. Zhu and S. Granick, *Phys. Rev. Lett.*, 2002, **88**, 106102.
65 O. I. Vinogradova, *Langmuir*, 1995, **11**, 2213–2220.
66 O. I. Vinogradova, *Langmuir*, 1996, **12**, 5963–5968.
67 C. Cottin-Bizonne, A. Steinberger, B. Cross, O. Raccurt and E. Charlaix, *Langmuir*, 2008, **24**, 1165–1172.
68 D. Y. C. Chan and R. G. Horn, *J. Chem. Phys.*, 1985, **83**, 5311–5324.
69 J. N. Israelachvili, *J. Colloid Interface Sci.*, 1986, **110**, 263–271.
70 L. Suresh and J. Y. Walz, *J. Colloid Interface Sci.*, 1997, **196**, 177–190.
71 J. Y. Walz, L. Suresh and M. Piech, *J. Nanopart. Res.*, 1999, **1**, 99–113.
72 C. L. Henry, C. N. Dalton, L. Scruton and V. S. J. Craig, *J. Phys. Chem. C*, 2007, **111**, 1015–1023.
73 C. L. Henry, L. Parkinson, J. R. Ralston and V. S. J. Craig, *J. Phys. Chem. C*, 2008, **112**, 15094–15097.
74 R. S. Allan, G. E. Charles and S. G. Mason, *J. Colloid Sci.*, 1961, **16**, 150–165.
75 A. Steinberger, C. Cottin-Bizonne, P. Kleimann and E. Charlaix, *Phys. Rev. Lett.*, 2008, **100**, 134501.
76 A. Steinberger, C. Cottin-Bizonne, P. Kleimann and E. Charlaix, *Nat. Mater.*, 2007, **6**, 665–668.
77 P. J. Scales, F. Grieser and T. W. Healy, *Langmuir*, 1990, **6**, 582–589.
78 P. G. Hartley, I. Larson and P. J. Scales, *Langmuir*, 1997, **13**, 2207–2214.

